Transfer Lines

W. Bartmann
CERN, Geneva, Switzerland

Abstract

Transfer lines are used to connect accelerators or deliver beam to fixed target experiments. In the following sections the design steps of a transfer line are introduced, starting from back-of-the-envelope calculations. The second part focuses on matching tools for optics design and related hardware specifications. The third part collects special topics which can appear in beam lines.

Keywords

CAS; transfer lines; optics matching; error and correction studies.

1 What is a Transfer Line?

The difference between rings and transfer lines was introduced in [1]. Let us recall that in a ring the condition of periodicity defines a unique solution for the Twiss parameters at any location along the accelerator. In a transfer line instead, without any condition of periodicity, the Twiss parameters are defined by the initial conditions and are propagated according to the transfer matrices of each element along the line. While the change of a single element in a ring, e.g. the tuning the strength of a quadrupole, will affect the optics all around the ring, the change will only be visible downstream of this element in a transfer line. Also, since beam passes only once a transfer line, hardware specifications with regard to field homogeneity, power converter stability and alignment are usually relaxed with respect to rings. On the other hand, it becomes more difficult and time consuming to measure beam parameters and align elements with beam. These uncertainties of the beam optics have to be taken into account in conservative margins for beam acceptances as detailed in the following sections.

2 Paper Studies

This section covers the initial design steps of a transfer line which are based on analytic calculations. They can be performed on paper and, most importantly, serve as an efficient crosscheck of studies performed with optics and tracking codes.

2.1 Geometry - estimate of bend angles

In order to calculate the geometry of a transfer line, coordinates and angles of the points to be linked have to be defined in a common coordinate system. While this is obvious for short lines of several meters, this has to be carefully performed for large scale accelerator systems, e.g linking CNGS to Gran Sasso in Italy where the CERN reference frame had to be connected to the global systems of Switzerland and Italy [2]. As soon as the geometry is defined, the required bending angles can be calculated from the magnetic rigidity

$$B\rho = \frac{p}{q} \qquad \rightarrow \qquad B\rho \, [Tm] = 3.3356 \, \frac{A}{n} \, p \, [GeV/c] \qquad (1)$$

where A is the atomic mass number, n the charge state and p the average momentum per nucleon. In case of electrostatic elements, the rigidity is written as

$$E\rho = \frac{pv}{q} \qquad \rightarrow \qquad E\rho \, [kV] = \frac{\gamma + 1}{\gamma} \, \frac{A}{n} \, T \, [keV] \qquad (2)$$

where T is the average kinetic energy per nucleon. The respective deflection angles are then:

$$\theta = \frac{Bdl}{B\rho} \quad or \quad \frac{Edl}{E\rho} \tag{3}$$

While the magnetic rigidity is proportional to the particle momentum, the electric rigidity is proportional to the kinetic energy. This behaviour, together with the technological limits of magnetic and electric bends, defines the energy reach of an accelerator. Electric devices are limited by the applied voltage. For reasonable accelerator apertures, several tens of kV can be assumed as limit. Magnets on the other hand are limited by the field quality at low fields. Due to the strong dependence on material properties, remnant fields become important and measuring the field becomes a challenge. A practical example where electric devices can be used to bend and focus the beam are the 100 keV antiproton beam lines for the antimatter factory at CERN. Here, electrostatic quadrupoles with a 60 mm diameter require applied voltages of below 10 kV, electrostatic bends of up to 30 kV. What are the criteria to choose between magnetic and electric elements if you are in this energy gray zone? Electric devices are cheap in production, have cheap power supplies and cables, they are mass-independent, have no hysteresis effects hence easy operation, no power consumption hence no cooling and the transverse field shape is easy to optimize. On the other hand, the field shape and effective length of electric devices is difficult to measure. Also the diagnosis of faulty connections can pose problems. In case these devices are inside vacuum, they present a large outgassing surface area, are vulnerable to dirt inside vacuum and require interlocking for sparking and safety. Any repair requires opening the vacuum and insulators have to be vacuum and bake-out compatible. Many of these arguments related to vacuum apply also to magnets.

Estimating the required bending angles can be straightforward as in the above mentioned example of 100 keV antiproton beam lines where the beam deflection in the is handled by single elements over a length of 0.5 m. Highly rigid beams require often long transfer lines due to the limit of maximum reachable magnetic fields. Here the bending is distributed over the full line and in first paper estimates one has to account also for focusing, diagnostic and vacuum elements. A reasonable dipole filling factor is around 70%.

So far we discussed technological limits of the bending fields. A few 10 kV can be applied on electric devices due to sparking. For magnets one can assume 2 T for normal conducting, iron dominated magnets and around 9 T for superconducting ones. But there are limits also coming from the beam itself. When H^- ions are transferred through a line with magnetic fields, the moving ions will see the magnetic field in its rest frame. The Lorentz transform of this magnetic field gives an electric field which can be written:

$$E \left[\frac{MV}{cm} \right] = 3.197 \cdot p \left[\frac{GeV}{c} \right] \cdot B\,[T] \tag{4}$$

The electric field can detach the extra electron with 0.755 eV binding enery which leads to a definition of the ion's lifetime:

$$\tau = \frac{A}{E} \exp^{\frac{C}{E}} \qquad A = 7.96 \cdot 10^{-14}\ s\ MV/cm,\ C = 42.56\ MV/cm \tag{5}$$

For the example of a 4 GeV H^- injection a reasonable fractional loss of less than 10^{-4} limits the magnetic field to 0.13 T, see Fig. 1. In case of the Fermilab Project-X study, it was considered to inject a 8 GeV H^- beam into the recycler [4]. While usually power loss limits in lines are assumed to about 1 W/m, the corresponding activation was found to be not acceptable for 8 GeV ions and therefore the power loss maximum reduced to 0.05 W/m. In this low loss regime, black body radiation appeared to give a relevant contribution. In Fig. 2, the H^- photo-detachment cross section is shown together with the black body spectrum at different energies. Figure 3 shows the power loss due to black body radiation as a function of the beam pipe temperature. Another effect relevant for very low loss levels is rest gas stripping for which the power loss per length l can be calculated as

$$P = E\,I\,\frac{d\sigma}{d\Omega}\,\rho\,l \tag{6}$$
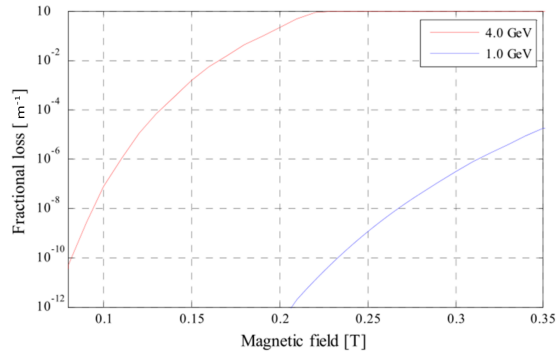
Fig. 1: Fractional loss of 1 and 4 GeV H$^-$ as a function of the magnetic field
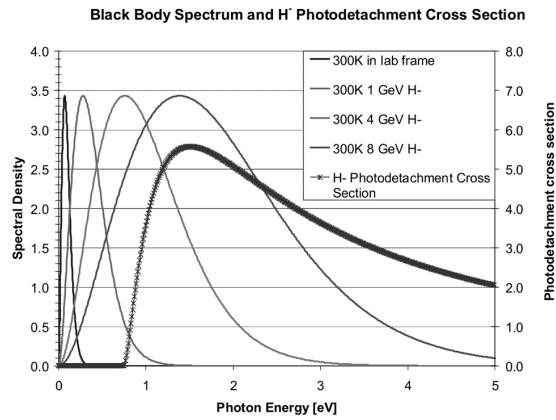
Fig. 2: Black body spectrum and H$^-$ photo-detachment cross section as a function of the photon energy [4]

where E and I denote the beam energy and density, respectively. ρ is the gas density which is a function of temperature and pressure. The gas dependent stripping cross sections show an electron loss behaviour proportional to $1/\beta^2$:

$$\frac{d\sigma}{d\Omega} = \frac{7 \cdot 10^{-19}}{\beta^2} cm^2 \qquad \text{per atom of nitrogen or oxygen}$$

$$\frac{d\sigma}{d\Omega} = \frac{1 \cdot 10^{-19}}{\beta^2} cm^2 \qquad \text{per atom of hydrogen}$$

(7)

All three effects, Lorentz stripping, black body radiation causing H$^-$ photo-detachment and rest gas stripping exceeded the acceptable loss level for the 8 GeV H$^-$ beam transport study. As a solution a cold beam screen (77 K) was assumed to reduce the photo-detachment cross section and the rest gas stripping. In order to limit Lorentz stripping, the magnetic field had to be below 0.05 T.

2.2 Focusing structure - estimate of quadrupole gradients

In case beam is extracted from a synchrotron, the focusing structure of the respective transfer line can be well defined already on paper. The cell length of a ring is usually optimized for the dipole filling at high energy. Therefore this cell length can be assumed well optimized also for the transfer line. Another assumption can be taken on the focusing structure and phase advance of each cell. Often a 90° FODO cell is used since it has a good ratio of minimum and maximum betatron functions, features equal aperture
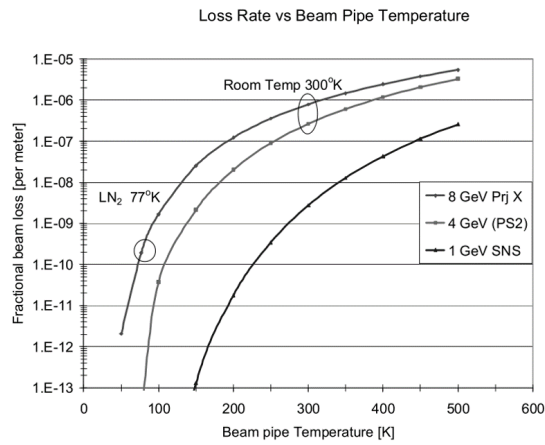
Fig. 3: Loss rate due to black body radiation for different beam screen temperatures [4]

requirements in both planes, provides good locations for trajectory correction and beam instrumentation and it provides the ideal phase advance for injection and extraction equipment. With the above taken assumptions on cell length and phase advance, the number of transfer line quadrupoles and their main parameters can be fully defined. The main quadrupole parameters are the pole tip field and radius, and
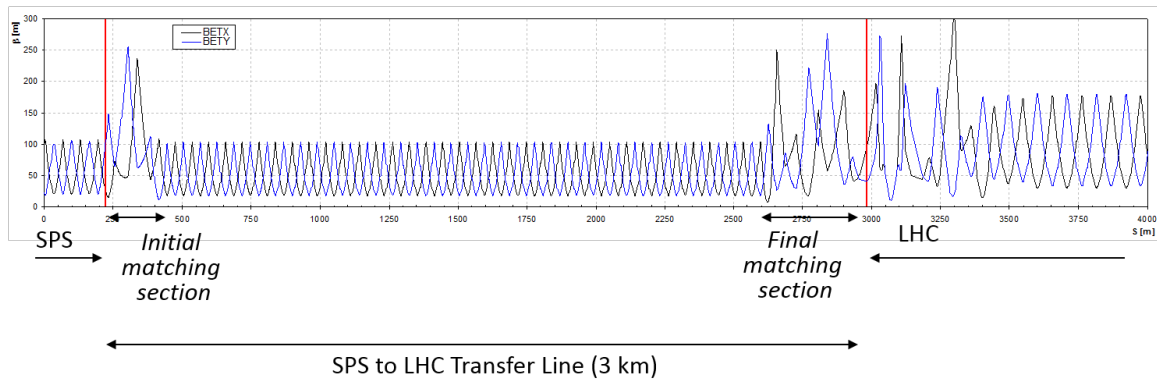
Fig. 4: Typical optics of a transfer line with a regular FODO structure and two matching sections on either side to connect to the respective ring optics'.

the gradient:

$$B = g \cdot x \qquad B_{poletip} = g \cdot a \tag{8}$$

Our assumptions on cell length and phase advance allow us to calculate the required quadrupole gradient. The transfer matrix for a 90° FODO cell, from centre to centre of two successive defocusing quadrupoles
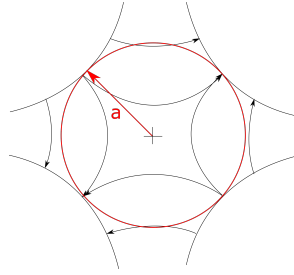
Fig. 5: Quadrupole pole tip radius

as shown in Fig. 6, can be written as:

$$R = \begin{pmatrix} 1 & 0 \\ 1/2f & 1 \end{pmatrix} \begin{pmatrix} 1 & L/2 \\ 0 & 1 \end{pmatrix} \begin{pmatrix} 1 & 0 \\ -1/f & 1 \end{pmatrix} \begin{pmatrix} 1 & L/2 \\ 0 & 1 \end{pmatrix} \begin{pmatrix} 1 & 0 \\ 1/2f & 1 \end{pmatrix}$$

$$= \begin{pmatrix} 1 - L^2/8f^2 & L - L^2/4f \\ -L/4f^2 - L^2/16f^3 & 1 - L^2/8f^2 \end{pmatrix} \tag{9}$$

$$= \begin{pmatrix} \cos\mu + \alpha\sin\mu & \beta\sin\mu \\ -\gamma\sin\mu & \cos\mu - \alpha\sin\mu \end{pmatrix}$$

From Equ. 9 we get

$$\frac{L}{f} = 4\sin\frac{\mu}{2} \tag{10}$$

Stability of such a FODO cell is given for

$$f > \frac{L}{4} \tag{11}$$

which is visualized in Fig. 6. For a 90° phase advance the focal strength becomes $f = \frac{L}{2\sqrt{2}}$. From
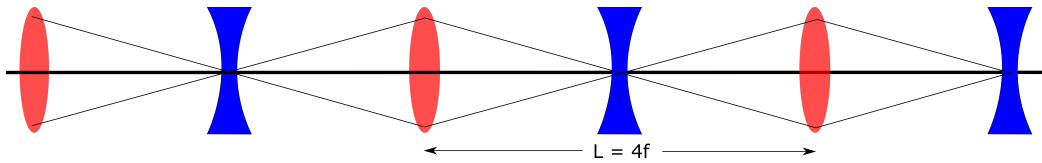
Fig. 6: FODO cell with stability condition [9]

the cell length, phase advance and the stability criterion we can define the quadrupole gradient and the maximum betatron functions:

$$\beta = \left(L + \frac{L^2}{4f} \right) / \sin\mu \tag{12}$$

In order to also estimate the pole tip field, the minimum inscribed radius inside the poles is needed. Specifying the acceptance of hardware elements in a transfer line requires to take into account certain margins in addition to the pure beam size. The following aperture formula for the radius can serve as example:

$$A_{x,y} = n_\sigma \sqrt{k_\beta \, \beta_{x,y} \, \frac{\epsilon_{x,y}}{\beta\gamma_{rel}}} + k_\beta \, D_{x,y} \, \frac{\Delta p}{p} + CO\sqrt{\frac{\beta_{x,y}}{\beta_{max}}} + alignment \tag{13}$$

The first two summands account for betatron and dispersive beam sizes, respectively. Those contributions are added linearly to stay more conservative when specifying hardware acceptances. The quadratic addition should be chosen when beam sizes are calculated for collimators and beam stoppers where the energy density on the material is critical. For the momentum spread it is advisable to use twice the rms value on the radius to include a reasonable part of this one-dimensional distribution. The third summand accounts for trajectory variations. Since their cause is often a dipole kick as $\Delta x = \Theta \sqrt{\beta_1 \, \beta_2} \, sin\Delta\mu$, the constant CO is scaled with the betatron function. The last contribution stands for misalignment or material roughness and is $\mathcal{O}(mm)$. The safety factor k_β stands for beta beating or more generally uncertainty in the optics. As a typical optics uncertainty 20% can be assumed. Depending on the beam energy and consequences of beam impact, the constant n_σ is often chosen to be around 3 in low energy beam lines and around 6 in high energy beam lines. With this aperture calculation the input is complete to specify fields and pole distances of dipoles and quadrupoles.

2.3 Alignment and field errors

Another important ingredient for designing magnets are maximum tolerances on the field errors. The impact of field errors on aperture requirements is usually very low, but they are very relevant for beam quality and emittance growth. There is a rigorous derivation of field errors in [5] of which only the results are quoted here:

$$\epsilon_2 = \epsilon_1 + \frac{1}{2}\left((\Delta y)^2 \frac{1+\alpha^2}{\beta} + \left(\Delta y'\right)^2 \beta\right) \tag{14}$$

ϵ_2 denotes the resulting emittance after taking into account magnet misalignments Δy and field errors $\Delta y' = \frac{\Delta Bl}{B\rho}$. Gradient errors from quadrupoles $k = -\frac{\Delta Gl}{B\rho}$ lead to an emittance growth as:

$$\epsilon_2 = \frac{1}{2}\left(k^2\beta^2 + 2\right)\epsilon_1 \tag{15}$$

For a given emittance growth budget, these estimates allows to specify the maximum tolerable field errors. Since there are usually many error sources, one has to average of these distributed errors:

$$\left\langle y^2 \right\rangle = \frac{\beta(s)}{2} \sum_n \beta_n \left\langle \delta_n^2 \right\rangle \tag{16}$$

with δ_n denoting the dipole and gradient errors as:

$$\delta_n = \frac{\Delta Bl}{B_0 \rho_0} \qquad and \qquad \delta_n = -lk\Delta y \tag{17}$$

which can be averaged using the rms error to:

$$\left\langle y^2 \right\rangle = \frac{\beta_{aver} \, n \, \delta_{rms}}{2} \tag{18}$$

It should be noted that this approach assumes uncorrelated errors along the transfer line. While this is a reasonable assumption for misalignments, errors related to powering are often strongly correlated, as can be seen in Fig. 5 where most of the quadrupoles are connected to the same power supply. Defining tolerances for misalignments and field errors is therefore more efficient via algorithms which will be shown in the following section. In order to roughly estimate the outcome of a correction study some ballpark figures are given below:

- – Number of monitors and required resolution
    - – Every $1/4$ betatron wavelength
    - – Grid resolution: 3 wires/σ

- Number of correctors and strength
  - Every $1/2$ betatron wavelength in H - same for V
  - Displace beam by few betatron σ per cell
- Dipole and quadrupole field errors
  - Integral main field known to better than 1 - 10^{-4}
  - Higher order field errors $< 1\text{-}10^{-4}$ of the main field
- Dynamic errors from power converter stability
  - $1 - 10^{-5}$
- Alignment tolerances
  - 0.1 - 0.5 mm
  - 0.1 - 0.5 mrad

It should be noted that these values strongly vary depending on energy, intensity and machine purpose. They can be used as good guess starting point for error and correction studies as treated in the following section.

3   Matching tools

In the previous section we estimated bending angles, quadrupole gradients, cell length, phase advance and apertures. In this section we will go into more detail by using MADX as tool for optics matching and error studies.

3.1   Optics and survey matching

In order to calculate the survey coordinates of a transfer line, we need start and end points in all three coordinates x, y, z and the three angles θ, ϕ, ψ as defined in Fig. 7. Before getting a matching routine to
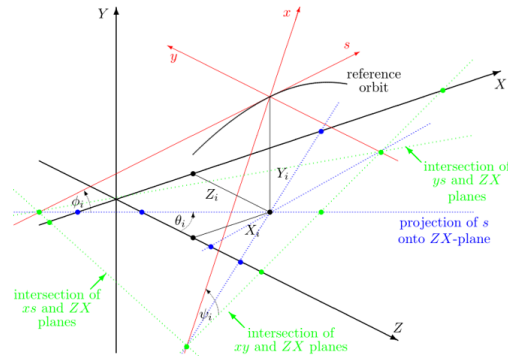
Fig. 7: MADX reference system [14]

calculate survey coordinates, a sequence of magnets needs to be established which is based on the paper estimates shown in the previous section. An example of such a line is shown in Fig. 8. This line has a central part with a FODO lattice and two matching sections on either side. There are two combined horizontal and vertical achromats. The first achromat is placed in the 90° FODO structure where the dispersion is canceled automatically if bends with the same angle are placed with 180° phase advance. In this example the dispersion of the second achromat is deliberately not fully canceled. Dispersion at the stripping foil is used to compensate for the Doppler spread particles with different momenta would
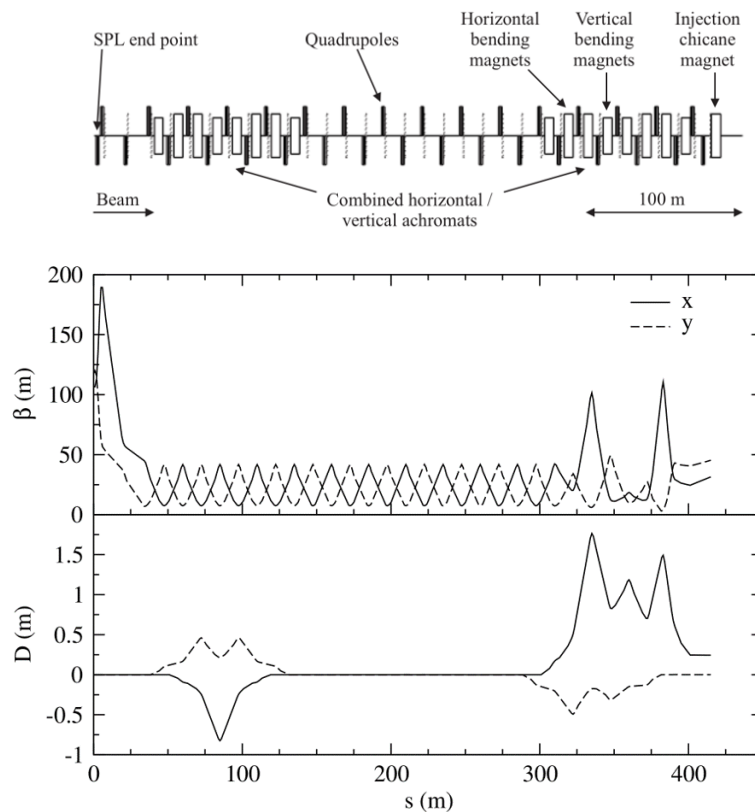
Fig. 8: Study of a transfer line between SPL and PS2 [6]

see and therefore not be excited by the laser light, explained in more detail in [1]. The related survey matching of this line is shown in Fig. A.1. While matching geometries the path length - and with it the target location - is changing. Therefore, in this example the location of the stripping foil has to be matched simultaneously. In order to match the optics, a basic FODO cell is defined as shown in the following code example. The strength initialization of the quadrupoles is according to Eq. 10.

The matching from the SPL optics to the FODO structure and from the FODO to the PS2 optics is shown in Fig. A.3. The matching itself is straightforward as long as there are enough knobs, i.e. independently powered quadrupoles available. It is advisable to start generously with the number of variables to find an initial solution, which then can be optimized by reducing the number of quadrupoles used for matching. The matching should not only target a single optics solution, but provide tunability of the line in case of optics uncertainty or changes. Also, it is not always straightforward to get the optics constraints right. It is good practice to use mechanical handover points of which the positions are clearly defined. For the optics conditions one should make sure that the single turn optics at injection or extraction with all injection or extraction equipment (kickers and bumps) is calculated to correctly take the dispersion created by these elements into account.

3.2 Final focus matching

Matching a final focus is required for fixed target experiments and often requires a high flexibility in tuning the optics parameters at the target. While a FODO structure provides good properties to transfer the beam along a line, other structures like a doublet or triplet give more optics flexibility at the focal

point. The transfer matrix of a doublet with distance d between the quadrupoles can be written as [8]:

$$\begin{pmatrix} 1 & 0 \\ -1/f_2 & 1 \end{pmatrix} \begin{pmatrix} 1 & d \\ 0 & 1 \end{pmatrix} \begin{pmatrix} 1 & 0 \\ 1/f_1 & 1 \end{pmatrix} = \begin{pmatrix} 1+d/f_1 & d \\ 1/f_1 - 1/f_2 - d/f_1 f_2 & 1 - d/f_2 \end{pmatrix} \quad (19)$$

For equal quadrupole strength the matrix reduces to

$$R = \begin{pmatrix} 1+d/f & d \\ -d/f^2 & 1-d/f \end{pmatrix} \quad (20)$$

which gives the effective focal length of a doublet:

$$f^* = \frac{f^2}{d} \quad (21)$$

A doublet can be used to focus particle rays from point to parallel as shown in Fig. 9 For this condition
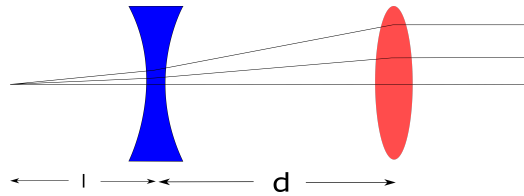
Fig. 9: Focusing particle rays point to parallel with a doublet structure

the matrix elements R_{22} and R_{44} need to be zero which gives

$$f_1\, f_2 = l\, d \qquad \frac{f_1}{f_2} = \frac{l}{l+d} \quad (22)$$

and for the magnetic fields:

$$f_1 = l\sqrt{\frac{d}{l+d}} \qquad f_2 = \sqrt{d(l+d)} \quad (23)$$

Now we can use two doublets to focus from point to point as shown in Fig. 10. By placing two mirrored
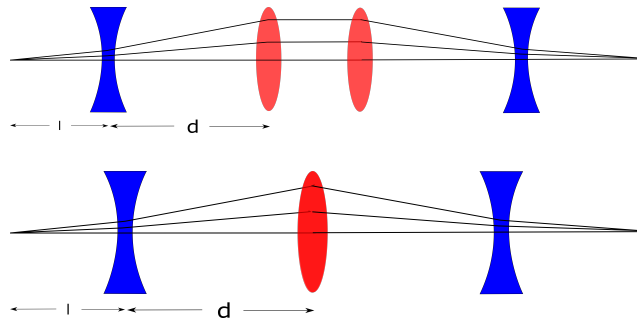
Fig. 10: Focusing particle rays point to point with a pair of doublets (top) which can be simplified to a triplet structure (bottom) [8].

doublets and combining the central quadrupoles into one we create a triplet structure. The corresponding transfer matrix is written as

$$R = \begin{pmatrix} 1 - 2\frac{d^2}{f^2} & 2d\left(1 - \frac{d}{f}\right) \\ -2\frac{d}{f^2}\left(1 + \frac{d}{f}\right) & 1 - 2\frac{d^2}{f^2} \end{pmatrix} \tag{24}$$

with the effective focal length

$$f^* = \frac{f^2}{2d}\left(1 + \frac{d}{f}\right) \tag{25}$$

With a triplet we can simultaneously control the focusing in both planes and create round spots on a target. Note that we could focus also with a single doublet point-to-point, but not symmetrically in both planes. The high optics flexibility of a triplet makes it the most common choice for final focus matching. In Fig. 11 we show the optics of a doublet and a triplet structure, respectively. Compared to a FODO, the doublet provides longer drift spaces for special equipment. Its betatron functions have steep asymmetric slopes. Triplets have distinct locations of high betatron functions but then allow to focus them down over long distances. These low betatron functions in the long drifts allow for small dipole apertures. Triplets also feature a high phase advance, e.g. for closing dispersion bumps. A typical example of a final
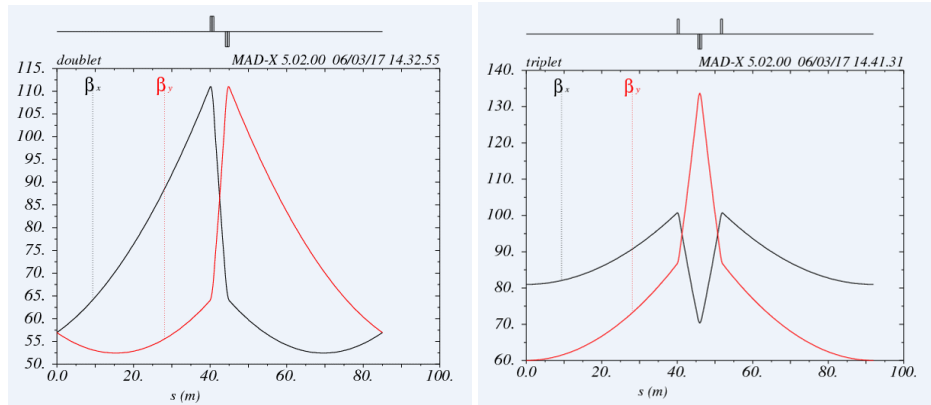
Fig. 11: Optics comparison of doublet (left) and triplet (right)

focus is shown in Fig. 12. The triplet structure upstream the experimental area not only allows to focus both planes to a round spot at the target location, but also the final focus can be shifted longitudinally. Also typical for the triplet optics are the large betatron peaks in the quadrupoles which often requires a dedicated large aperture magnet design.

3.3 Achromats

For many fixed target experiments it is beneficial that the trajectory be independent of the particle momenta and thus, dispersion is usually matched to zero at the focal point. Also for beam transfer between synchrotrons, dispersion in the injection and extraction regions is limited to $\mathcal{O}(10cm)$ to keep beam sizes small and in case of high energy beam transfer, protection system settings independent of momentum errors. In the following the optics conditions of an achromat are introduced. Let us consider two dipole magnets enclosing a quadrupole as shown in Fig.13. The transfer matrix of this system can be written as

$$M = \begin{pmatrix} 1 & 0 & 0 \\ -hs_2 & 1 & s_2 \\ 0 & 0 & 1 \end{pmatrix} \begin{pmatrix} 1 & L_2 & 0 \\ 0 & 1 & 0 \\ 0 & 0 & 1 \end{pmatrix} \begin{pmatrix} 1 & 0 & 0 \\ -1/f & 1 & s_2 \\ 0 & 0 & 1 \end{pmatrix} \begin{pmatrix} 1 & L_1 & 0 \\ 0 & 1 & 0 \\ 0 & 0 & 1 \end{pmatrix} \begin{pmatrix} 1 & 0 & 0 \\ -hs_1 & 1 & s_1 \\ 0 & 0 & 1 \end{pmatrix} \tag{26}$$
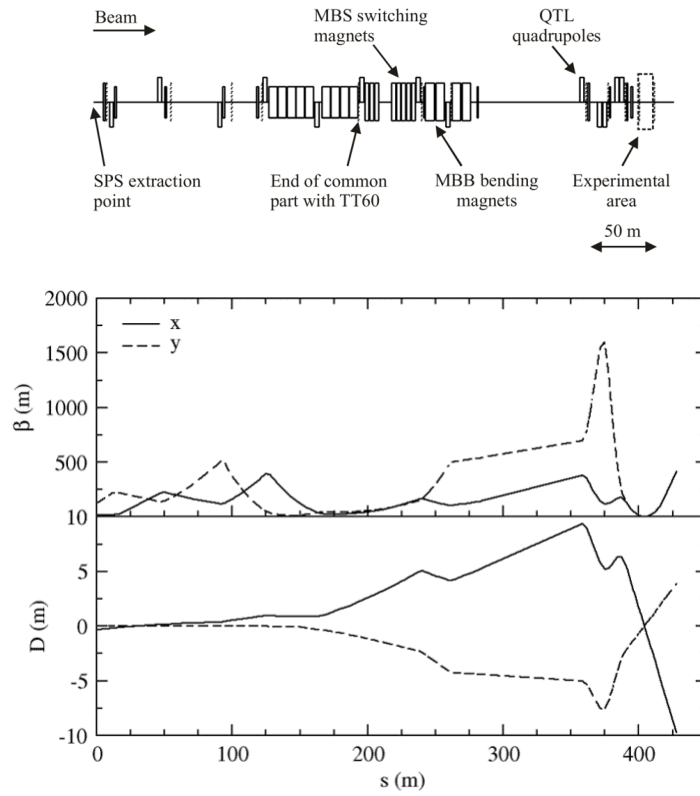
Fig. 12: Final focus optics of the material test facility HiRadMat at CERN [7]
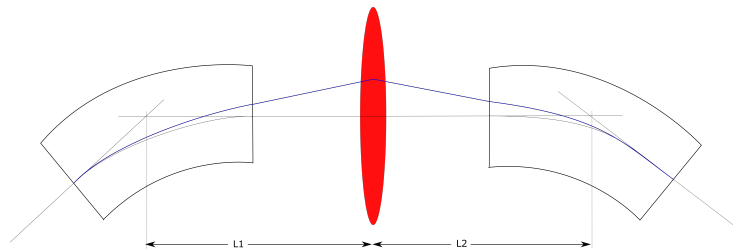
Fig. 13: Basic cell for definition of achromatic condition

with the following relations for the matrix of a single dipole:

$$R_{bend} = \begin{pmatrix} 1 & 0 & 0 \\ -hs & 1 & s \\ 0 & 0 & 1 \end{pmatrix} \quad \dots \quad h = \frac{B}{B\rho}, \; s = \sin\alpha \tag{27}$$

By multiplying Equ. 26 we get the relation for the dispersion and its derivative:

$$D_x = L_2 s_1 \left(1 - \frac{L1}{f} \right) + L_1 s_1$$
$$D'_x = L_1 s_1 \left(-h s_2 - \frac{1}{f} + \frac{h s_2 L_2}{f} \right) + s_1 \left(1 - h s_2 L_2 \right) + s_2 \tag{28}$$

For an achromat, both must vanish which defines the strengths and lengths parameters in our system to:

$$\frac{1}{f} = \frac{1}{L_1} + \frac{1}{L_2} \tag{29}$$

$$L_1 s_1 = L_2 s_2$$

Several achromat examples with point-to-point focusing are shown in Fig. 14. They are mostly used
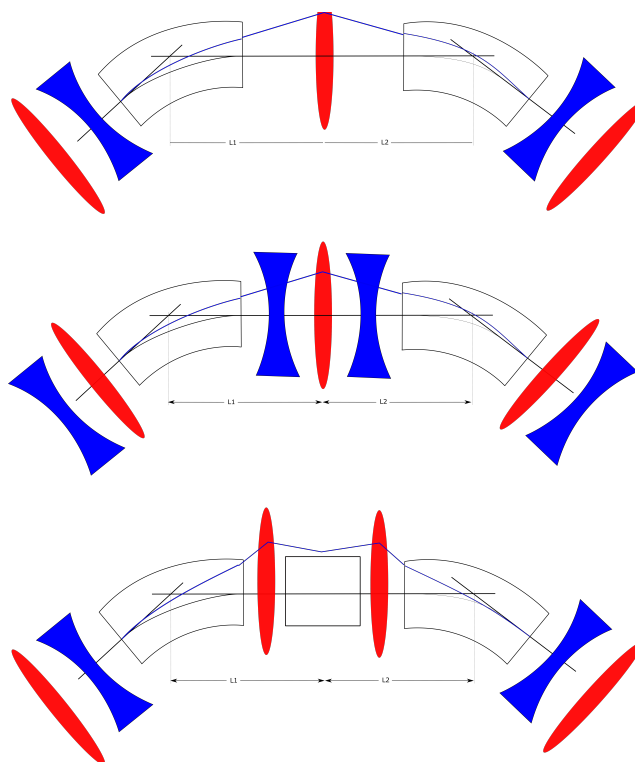
Fig. 14: Achromat examples with point-to-point focusing mostly used in high brightness machines. The double bend achromat (DBA) or Chasman-Green lattice (top), an expanded DBA (middle) and a triple bend achromat (bottom) [10].

in synchrotron light sources. For the Chasman-Green double bend achromat, the central quadrupole is focusing the dispersion down to zero at the outer ends of the dipoles and contributes little to the overall focusing. The quadrupoles outside the dipoles do not alter the dispersion behaviour, they solely provide focusing in both planes. A target placed in the centre can be used as a spectrometer. In contrary to the Chasman-Green lattice, there is strong focusing in the dispersive area for the expanded DBA and the triple bend achromat. For the latter two, one should consider installing sextupoles for chromaticity correction.

3.4   Error and correction studies

After having designed a first order optics for our beam transfer, we need to go a step deeper and evaluate this design against different kinds of errors. In a first step we need to define tolerable error levels in the transfer line. This can be a loss level in W/m, percentage of beam lost or activation level, the trajectory offset in position and angle at the point of delivery, the shot-to-shot and long term variation of the trajectory and the optics, rotation or energy mismatch at the point of delivery. As second step we need to assume reasonable errors for the hardware and study their impact. The error input needs then to be iterated until an acceptable level is reached, which allows then to specify the hardware accordingly.

Usually the error assignment in a transfer line starts from the input error which is defined by the preceding machine. In Fig. A.4 an example is given on how to distribute an assumed or measured orbit offset at extraction according to the optics at the transfer line start. As a next step, magnets in the transfer line need to get errors assigned as shown in Fig. A.5. There are different ways of defining a field error, and in the following we will discuss the multipole expansion of the static magnetic field used in MADX and most other optics codes:

$$B_y + iB_x = B_{ref} \sum_{n=1} (b_n + ia_n) \left(\frac{x + iy}{R_{ref}^{n-1}} \right)^{n-1} \tag{30}$$

where b_n, an, are normal and skew multipole coefficients. R_{ref} is the reference radius, and B_{ref} an appropriately chosen normalization. For a long magnet, the vector potential A in the magnet aperture has only the longitudinal component $A(0, 0, Az)$, with:

$$A_z = -B_{ref} \sum_{n=1} (b_n + i\,a_n) \frac{Re\,(x + iy)^n}{n\,R_{ref}^{n-1}} \tag{31}$$

The Hamiltonian then directly contains the multipole coefficients:

$$H(x, y, z, t) = q\phi + \sqrt{\left(\frac{p_z - qA}{1 + k_x x} \right)^2 + p_x^2 + p_y^2 + m^2 c^4} \tag{32}$$

The multipole expansion is analytical and satisfies automatically the equations for the static field in 2D. It is based on a a complete and orthogonal set of basis functions which means that the values of the low order multipoles do not depend on the number of terms included in the expansion. This is important for the precision of dipole, quadrupole and sextupole fields which do not change if the series contains 8 or 10 terms for example. The expansion guarantees convergence for all radii within the reference radius. On a more practical term, the expansion on a circle is well matched to the rotating coil technique which allows for low measurement and low data treatment errors. If the aperture is very asymmetric as in classical dipoles, the multipole expansion can be performed on an elliptical boundary. Circular and elliptical multipoles are related by a linear transformation. The term "Good Field Region" is a concept related to iron-dominated dipole magnets, with an implicit assumption that the field deviations are largest at the borders of the region near the pole. Here field plots are often fitted with a polynomial, which is however not an orthogonal set and does not necessarily satisfy the field equations. While this polynomial representation can be very useful for magnet design, the multipole expansion should be used to translate field errors into beam impact in optics codes. Which field errors do we need to consider in transfer lines? For the linear terms the dipole and quadrupole strengths are relevant, including power converter errors, transverse misalignments and rotations. As first non-linear term, the normal sextupole can be included. These errors affect the emittance growth, rms orbit errors, and chromatic properties of the transfer lines. The field in the measured or calculated aperture should be obtained on the largest possible reference radius R_{ref}. Ballpark figures as mentioned in Section 2.3 can be used as a good guess starting point. As soon as these distributed errors are assigned to all relevant elements

in the line, the impact on the beam can be simulated as shown in Fig. 16. The level of the trajectory distribution before correction is relevant for first setup of a beam. Trajectory correction is then based on small independently powered dipoles (correctors) and instrumentation to measure the position response downstream of the corrector. Horizontal and vertical correction elements are separated according to
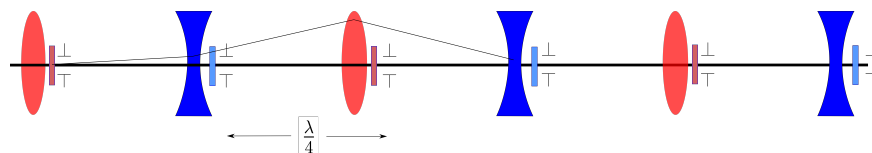
Fig. 15: Setup of correctors and monitors in a FODO lattice

locations of high betatron functions while position pick-ups should be located every quarter of a betatron wavelength as shown in Fig. 15. Special care has to be taken to avoid π-bumps. In case a correction is calculated with many disabled monitors and therefore a poor sampling of phase space, a large trajectory excursion can be created by the correction algorithm. Sufficient instrumentation is therefore essential for trajectory correction. The required correction level is depending on the location in the line. A global correction can be used to minimize the rms offsets at the monitors using all or some of the available correctors. Steering in matching sections and injection and extraction regions requires particular care due to large optics and dispersion functions, limited aperture, losses at collimators and injection offsets being detrimental for performance, i.e. emittance growth. A correction example in MADX is shown in Fig. A.6. One should be careful when running through a loop of many corrections that the corrector kicks are not adding up. As output of such a study it is useful to display trajectories before and after correction and compare to what one is including as trajectory contribution $CO \cdot \sqrt{\frac{\beta}{\beta_{max}}}$ in the aperture specification in Equ. 13. While trajectory offsets in a transfer line are acceptable as long as the beam
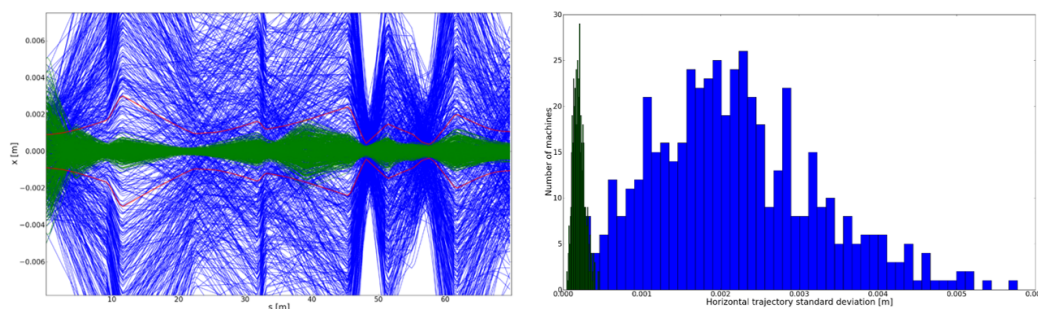
Fig. 16: Trajectories before and after correction (left), the red envelope shows the corresponding contribution in the aperture specification. Distribution of trajectories as a function of maximum offset along the line (right).

envelope does not exceed the good field region of magnets, it is more critical at the end of a line when the beam is delivered onto a target or injected into another machine. In order to perform statistics on the error distribution at the handover point, it is useful to express the error in form of the displacement vector D in normalized phase space as shown in Fig. 17. From this the correlated emittance growth due to filamentation can be directly estimated as:

$$\epsilon_2 = \epsilon_1 + \frac{1}{2}D^2 \tag{33}$$

The next step is a sensitivity analysis to identify the most important contributions to the deliver impreci-
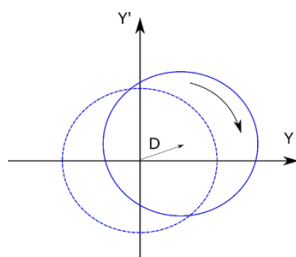
Fig. 17: Displacement vector in normalized phase space

sion and accordingly adjust specifications. This also includes instrumentation errors where the result of the study should define the severeness of reading, scaling and full failure errors. Most synchrotrons use a transverse feedback system to damp injection oscillations. The damping effect of the feedback on the emittance growth can be estimated as:

$$\epsilon_2 = \epsilon_1 + \frac{1}{2}\left((\Delta y)^2\frac{1+\alpha^2}{\beta} + (\Delta y')^2\beta\right)\left(\frac{1}{1+\tau_{DC}/\tau_d}\right)^2 \tag{34}$$

where τ_{DC} and τ_d denote the decoherence and damping time, respectively. So far we can specify the peak oscillation amplitude to be damped and the damping time. The required bandwidth of the feedback system needs to be estimated from an FFT analysis of the powering waveforms of the most important error contributions.

4 Special topics in transfer lines

This section focuses on specific topics in transfer lines like particle tracking, perturbation from stray fields, emittance exchange, deflection on a slope and dilution for dump systems.

4.1 Particle tracking

Particle tracking is mostly used to study amplitude dependent impact of non-ideal magnetic fields onto the beam. In particular if special elements are used which are not built-in elements in the code, simulated or measured field maps can be used to track particles through. From the resulting particle distribution the transfer matrix of the special element can be fitted and used as input for an optics code. A real example of this approach is the design of the 100 keV antiproton transfer lines at the Extra Low Energy Antiproton ring at CERN. Due to the low energy transfer lines, electrostatic elements are used to bend and focus the beam. A first order optics was established with MADX and then field maps of strong bending elements were simulated. Particles were tracked through these field maps and the Twiss parameters representing the transfer through the field map were then evaluated from the statistical distributions shown in Fig. 18. In Fig. 19 the optics of a full line tracking is compared to the optics from MADX where quadrupoles are used as built-in elements and bends as transfer matrices. At the end of the line a difference in optics functions can be seen which is due to the hard-edge approximation in MADX which is most visible in the location of the final focus where gradients are strongest.

Another example of particle tracking at beam transfer is the quantification of tail population due to mis-kicked bunches at the SPS injection. The batch spacing required for ions is shorter than the kicker rise time which leads to different deflections of a few bunches at the beginning and end of a batch. To a big part this oscillation can be damped with the transverse feedback and there is no measurable growth of emittance. However, an increased population of the transverse bunch tails is observed by loss
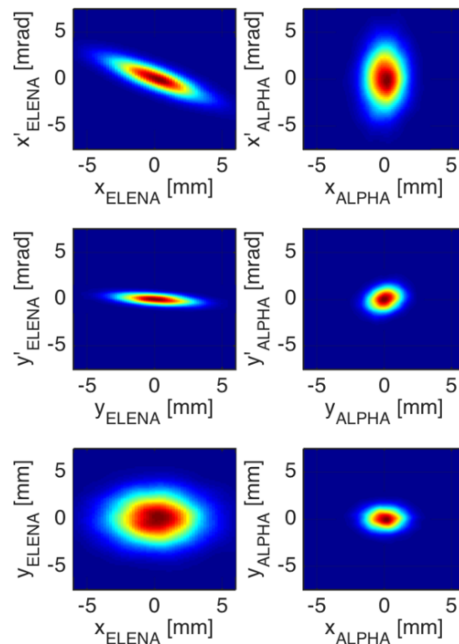
Fig. 18: Phase space distributions of tracked particles at the end of the ELENA ring (left) and the experiment focal point (right) [11].
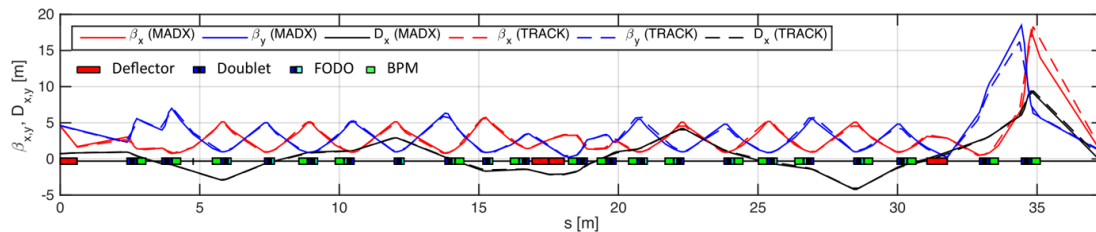
Fig. 19: Optics functions from the ELENA ring to the experimental focal point [11]

measurements on transfer line collimators. In order to simulate this effect, the motion through the SPS ring was described by the effective Hamiltonian formalism [13] where Lie algebra is used to establish a One Turn Map. At turn zero particles get an injection error and in later turns they receive a damping effect from the transverse feedback. In order to establish the coefficients of the effective Hamiltonian, the amplitude dependent detuning needs to be measured in the ring. The chromatic terms and the damper gain are estimated from decoherence measurements as shown in Fig. 20. Figure 21 shows the particle displacement after several thousands of turns for different cases of mis-kick. The gray shaded element stands for the collimator where the displaced particles can be measured as losses.

4.2 Stray fields

A different problem in transfer lines are stray fields which can deteriorate the beam quality or even cause full beam loss. The above mentioned antiproton lines lead a 100 keV beam to several experiments which
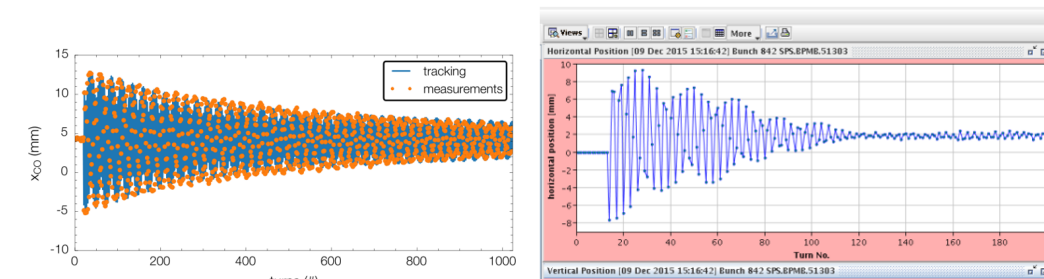
Fig. 20: Measurement and tracking results of amplitude dependent detuning (left) and decoherence measurements (right), courtesy F.M. Velotti.
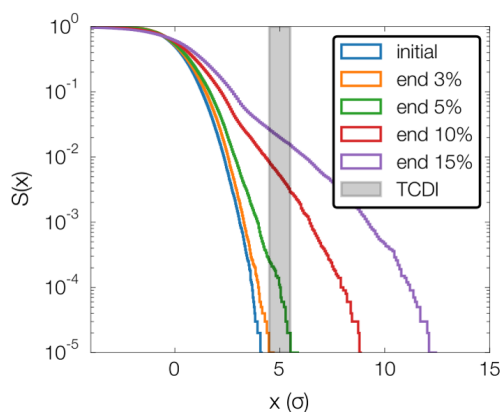
Fig. 21: Particle displacement after several thousands of turns, courtesy F.M. Velotti

have solenoids of up to 5 T field. In order to estimate the impact of these solenoid stray fields onto the beam, the solenoids' magnetic field is modeled with an analytic description of current loops and the integrated transversal fields are translated along the beam line into horizontal and vertical kicks. The resulting effect on the beam trajectory is shown in Fig. 22. The straight lines show the available aperture, which means that trajectory correction is required to stay within the available aperture. Stray fields can be attenuated with magnetic shielding and in Fig. 23 it is shown that a factor 50 attenuation is required to allow for an rms trajectory correction of 10^{-5} m. In case one needs to be independent of different solenoids ramping their fields simultaneously, an attenuation factor of 800 is needed.

The measured field might contain also quadrupolar or higher components. These can be taken into account as multipole kicks in MADX. In case of the PS injection, the stray field of the PS main combined function magnet units was measured and translated into multipole kicks every 2 cm along the last meters before injection.

4.3 Emittance exchange

Acceptances of circular accelerators tend to be larger in the horizontal plane in order to minimize as much as possible the bending dipole gap height. Several multiturn extraction processes produce however beams with emittances larger in the vertical plane. By exchanging the horizontal and vertical planes in a transfer line, we can inject a beam better matched to the acceptance of the downstream accelerator
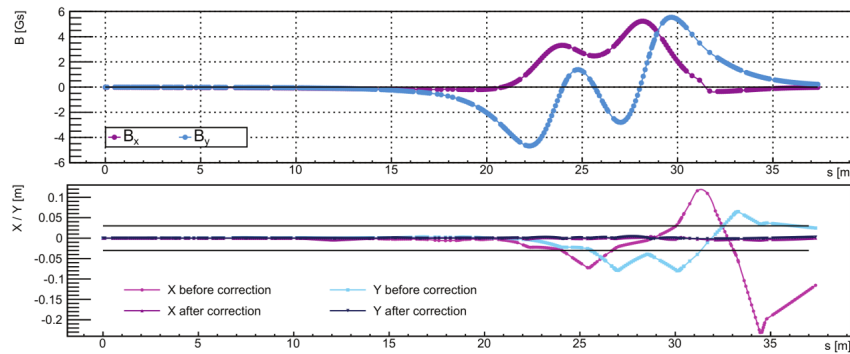
Fig. 22: Stray field level (top) and trajectory displacement (bottom) along the 100 antiproton transfer lines [12].
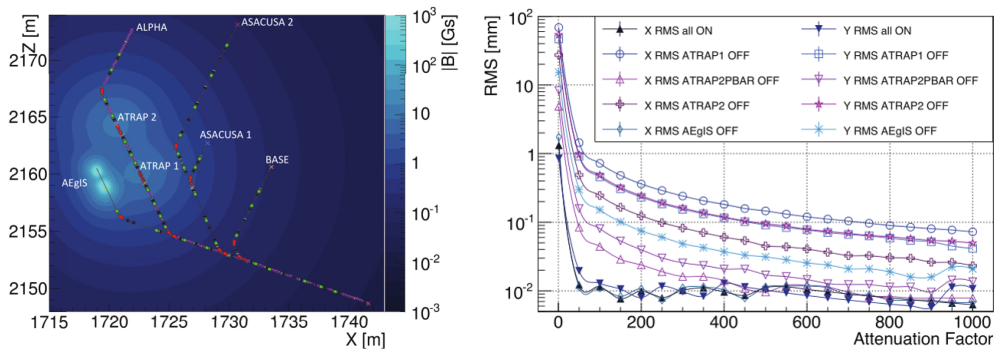
Fig. 23: Magnetic field map in the antiproton decelerator hall at CERN (left) and the respective rms trajectory variation as a function of magnetic shielding attenuation factor [12].

and such, reduce losses at the injection process, see Fig. 24. Skew quadrupoles, which are normal
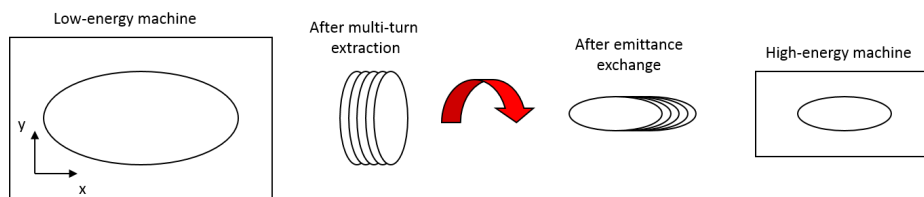
Fig. 24: Emittance exchange to reduce losses in downstream accelerators [3]

quadrupoles rotated by 45°, introduce a rotation into the beam. A rigorous derivation of this rotation can be found in [5]. The simplest result for a 90° FODO lattice is given by three skew quadrupoles, each separated by 90° phase advance, see Fig. 25 and a focal strength of:

$$\delta_{skew} = \frac{1}{\sqrt{\beta_x \beta_y}} \tag{35}$$
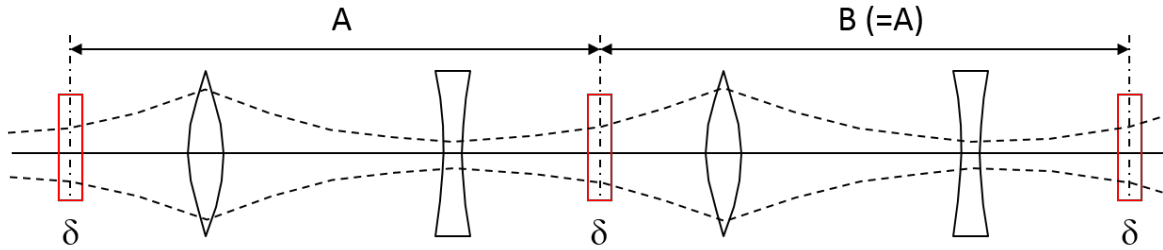
Fig. 25: Emittance exchange insertion with three skew quadrupoles in a 90° FODO lattice [3]

4.4 Tilt on a slope

In the previous section we have seen that skew quadrupoles can tilt beams around their longitudinal axis. The same effect occurs in a transfer line where e.g. a horizontal dipole is installed on a vertical slope [15]. The resulting tilt amounts to

$$\psi = \alpha \, \phi \tag{36}$$

where α and ϕ denote the bend and the slope angles, respectively. From a single dipole, this effect is small and in the order of misalignment, but it becomes significant when accumulated over many dipoles over a long transfer line. In case of the LHC transfer line TI 8 the roll angle accumulates to 65 mrad. LHC itself is inclined but usually we calculate rings as if they were located in the x-z plane and the survey becomes 2D, thus, tilt and roll angle are zero. If one considers the LHC inclination, the tilt and roll angle oscillate but are perfectly closed after one turn:

$$\phi_{max} \, cos\theta \qquad ... \qquad \phi_{max} = 14.04 \, mrad \tag{37}$$

At the injection point, LHC has a local tilt angle of 13 mrad which is not matched to the tilt at the end of TI 8. The corresponding emittance growth is negligible with about 1% for LHC. In general one should match trajectories in all six geometric degrees of freedom. MADX is correctly taking into account the roll angle calculation for dipoles on a slope, however, one needs to make sure to calculate also for a ring the local tilt at the injection point as matching target.

4.5 Dilution

Beam dilution needs to be applied if the deposited energy of the full beam is above the damage limit of dumps or targets. Hydrodynamic tunneling tests at the HiRadMat facility at CERN showed that the LHC beam - if not diluted - would drill a hole of about 35 m length into copper. For an undiluted FCC beam the length of the hole would become around 300 m in copper [16]. For certain targets it is sufficient to blow up the beam size to reduce the energy density in the material. In case of LHC and FCC this would lead to unfeasible absorber dimensions. Instead one is using time-varying dipole fields which give each bunch a different deflection and therefore distribute the particle density on the absorber as shown in Fig. 26. This bunch pattern on the dump is the input to study the shower development inside the block as discussed in [17].

5 Conclusions

In the previous sections we went through the design steps of a transfer line. It is revealing how far such a design can lead on paper. One can define the number of dipoles, quadrupoles, correctors and monitors with great accuracy. Also dipole and quadrupole fields as well as their apertures can be defined. Even
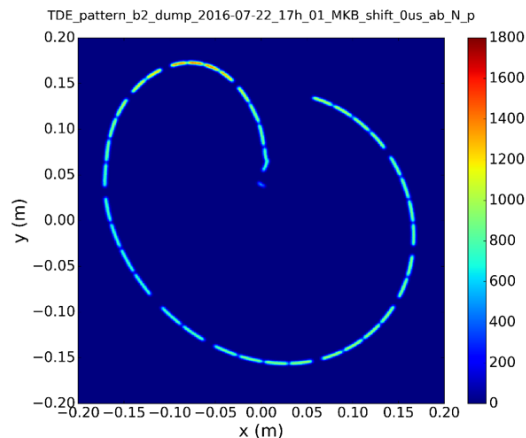
Fig. 26: Bunch pattern on the LHC dump block

a rough estimate of the required field quality and alignment accuracy is possible before switching on a computer.

Error and correction studies, however, show clearly the limits between paper studies and the need of deploying optics codes. We introduced with code examples how to calculate the optics for matching and final focus sections and this allowed to precise the field estimates from paper studies for quadrupoles and dipoles. We went through examples of error and corrections studies to define misalignment tolerances, field homogeneity and ripple, specifications of transverse feedback systems and sensitivity of instrumentation.

For certain cases it is required to dig deeper and track particles, e.g. numerical particle tracking through field maps in case we want to use elements which are not built-in to our codes or for the dedicated problem of transverse tail population due to injection error. We saw problems of transfer lines on the energy extremities as stray field calculation and mitigation in case of 100 keV antiproton lines next to 5 T solenoids or the need for diluting the beam in the high energy dump lines as for LHC and FCC.

6 Acknowledgement

Appendices

A MADX code examples

References

[1] B. Goddard, Introduction to Beam Transfer, these proceedings, CAS (2017).

[2] N. Ibarrola and M. Jones, Analysis and Evaluation of the CERN Reference Systems, International Workshop of Accelerator Alignment, ((2016)

[3] B. Goddard, Transfer lines, CAS (2004).
http://cas.web.cern.ch/cas/Baden/PDF/transfer.pdf

[4] D. Johnson, Challenges associated with 8 GeV H- Transport and Injection for FERMILAB PROJECT X, Proceedings of Hadron Beam 2008, (2008)

[5] P. Bryant, Beam Transfer Lines, CAS, (1992) `http://cds.cern.ch/record/261067?ln=en`

[6] C. Hessler et al., Transfer Lines to and from PS2, IPAC, Japan, (2010).
`https://cds.cern.ch/record/1277940/files/sLHC-PROJECT-REPORT-0043.pdf`

[7] C. Hessler et al., Beam Line Design of the HiRadMat Test Facility, EuCARD-CON-2009-053, (2009).
`https://cds.cern.ch/record/1307570/files/EuCARD-CON-2009-053.pdf`

[8] D. Carey, The Optics of Charged Particle Beams, (1987)

[9] J. Rossbach and P. Schmueser, Basic Course on Accelerator Optics, CAS, (1992) `http://cds.cern.ch/record/247501?ln=en`

[10] P.J. Bryant and K. Johnsen, The Principles of Circular Accelerators and Storage Rings, (1993).

[11] M. Fraser, Beam Dynamics Studies of the ELENA Electrostatic Transfer Lines, CERN-ACC-2015-340, (2015).
`https://cds.cern.ch/record/2141774`

[12] J. Jentzsch et al., Beam Dynamics Studies of the ELENA Electrostatic Transfer Lines in the Presence of Magnetic Stray Fields, Proceedings of IPAC2016, Korea, (2016),
`https://cds.cern.ch/record/2207454/files/thpmb047.pdf`

[13] W. Herr, Mathematical and Numerical Methods for Non Linear Beam Dynamics in Rings, CAS, (2013).

[14] L. Deniau, The MAD-X Program, CERN, (2017) `http://cern.ch/madx/releases/last-rel/madxuguide.pdf`

[15] B. Goddard et al., Geometrical Alignment and associated beam optics issues of transfer lines with horizontal and vertical deflection, LHC Project Report 719, (2004).
`https://cds.cern.ch/record/733786/files/lhc-project-report-719.pdf`

[16] F. Burkart, A. Piriz, R. Schmidt, A. Shutov, N. Tahir, D. Wollmann and M. Zerlauth, Experimental and Simulation Studies of Hydrodynamic Tunneling of Ultra-Relativistic Protons, Proceedings of IPAC2015, USA, (2015).
`http://inspirehep.net/record/1417473/files/mopty052.pdf`

[17] A. Lechner, Particel Interactions with Matter, these proceedings, CAS, (2017)

```
TITLE, 'TTL1';

// read in sequence file
OPTION, -ECHO, WARN, -INFO;
CALL,          FILE = "ttl1-v1.0.0.seq";

// read in beam properties
call, file = "beam.madx";

//---------------------- Survey matching to PS2 --------------------

USE,          SEQUENCE = TTL1;

// read in survey coordinates at the injection point (stripping foil)
// in the PS2 (real beam direction)
call, file = 'out.ps2foil-v8.0.4.survey.ini.mad';

value,          ps2.omk.foil.x0,
        ps2.omk.foil.y0,
        ps2.omk.foil.z0,
        ps2.omk.foil.theta0,
        ps2.omk.foil.phi0,
        ps2.omk.foil.psi0;

// define macro for position matching routine:
m1: MACRO={USE,          SEQUENCE = TTL1;
          SURVEY,
           x0 = -1510.09247,
                     y0 = 2423.58630,
                     z0 = 2278.25946,
                     theta0 = 0.8715909,
                     phi0 = -0.0150853,
                     psi0 = 0.0;};

// match position and angles at injection point (stripping foil):
MATCH, USE_MACRO;

//VARY, name = MB.v1.angle,   STEP = 0.001, LOWER = 0.01,  UPPER = 0.03;
VARY, name = MB.h1.angle,    STEP = 0.001, LOWER =-0.06,  UPPER =-0.01;
VARY, name = MB.h2.angle,    STEP = 0.001, LOWER =0.01,   UPPER = 0.06;
//VARY, name = MB.v2.angle,   STEP = 0.001, LOWER =-0.033, UPPER =-0.01;
VARY, name = ps2.omk.foil.at, STEP = 0.001, LOWER =400,    UPPER = 425;

USE_MACRO, name= m1;

CONSTRAINT,   expr= table(survey,ps2.omk.foil,x) = ps2.omk.foil.x0;
//CONSTRAINT, expr= table(survey,ps2.omk.foil,y)=ps2.omk.foil.y0;
CONSTRAINT,   expr= table(survey,ps2.omk.foil,z)=ps2.omk.foil.z0;
CONSTRAINT,   expr= table(survey,ps2.omk.foil,theta)=ps2.omk.foil.theta0;
//CONSTRAINT, expr= table(survey,ps2.omk.foil,phi)=ps2.omk.foil.phi0;
//CONSTRAINT, expr= table(survey,ps2.omk.foil,psi)=ps2.omk.foil.psi0;

LMDIF, CALLS:=5000, TOLERANCE:=1.E-10;
//JACOBIAN,  CALLS= 500, TOLERANCE= 1.0E-21;
ENDMATCH;
```

Fig. A.1: Example of survey matching code, courtesy C. Hessler

```
// FODO cell properties
l.fodo    = 25;
phadv     = pi/2.0;// 90deg phase advance per cell
k1.theo   = 4.0 / (l.mq * l.fodo) * sin(phadv/2.0);
value, l.fodo, phadv, k1.theo;

kqif.cell = k1.theo;//  5.98643e-02
kqid.cell =-k1.theo;// -5.98462e-02


//---------------------- Prototype Cell ----------------------

FCELL: SEQUENCE, L = l.fodo;

MQF.b:MQH,  AT := l.MQ/4,             K1 := kqif.cell;
MQD.a:MQH,  AT := l.fodo*0.5-l.MQ/4,  K1 := kqid.cell;
MQD.b:MQH,  AT := l.fodo*0.5+l.MQ/4,  K1 := kqid.cell;
MQF.a:MQH,  AT := l.fodo-l.MQ/4,      K1 := kqif.cell;

ENDSEQUENCE;

USE,   SEQUENCE = FCELL;
MATCH, SEQUENCE = FCELL;
  VARY, NAME = kqif.cell, STEP = 0.001, LOWER = 0.0, UPPER = mq.k1.max;
  VARY, NAME = kqid.cell, STEP = 0.001, LOWER = -mq.k1.max, UPPER = 0.0;
  CONSTRAINT, RANGE = #E, MUX = phadv/(2*pi), MUY = phadv/(2*pi);
LMDIF, CALLS:=5000, TOLERANCE:=1.E-10;
ENDMATCH;

SELECT,  FLAG=TWISS, COLUMN=NAME,S,BETX,BETY,ALFX,ALFY,DX,DPX,DY,DPY;
TWISS,   FILE = "fodo.twiss";
```

Fig. A.2: Example of matching a single FODO cell to 90° phase advance, courtesy C. Hessler

```
//---------------------- Match TTL1 to SPL -----------------------

USE,   SEQUENCE = TTL1;
MATCH, SEQUENCE = TTL1, VLENGTH = TRUE,
   BETX = BETX0, ALFX = ALFX0,
   DX   = DX0,   DPX  = DPX0,
   BETY = BETY0, ALFY = ALFY0,
   DY   = DY0,   DPY  = DPY0;
  VARY,  NAME = kqid.0, STEP = 0.001, LOWER = -0.1, UPPER = 0.0;
  VARY,  NAME = kqif.1, STEP = 0.001, LOWER = 0.0, UPPER = 0.1;
  VARY,  NAME = kqid.1, STEP = 0.001, LOWER = -0.1, UPPER = 0.0;
  VARY,  NAME = kqif.2, STEP = 0.001, LOWER = 0.0, UPPER = 0.1;
  CONSTRAINT,  RANGE = MQF.4, BETX = MQF.betx, BETY = MQF.bety;
  CONSTRAINT,  RANGE = MQF.4, ALFX = MQF.alfx, ALFY = MQF.alfy;
  //CONSTRAINT, RANGE = #E,      DX>-0.1, DX<0.1, DY>-0.1, DY<0.1;
  //CONSTRAINT, RANGE = #E,      DPX=0, DPY=0;
LMDIF, CALLS:=5000, TOLERANCE:=1.E-10;
ENDMATCH;

//---------------------- Match TTL1 to PS2 -----------------------

USE,       SEQUENCE = TTL1;
MATCH,        SEQUENCE = TTL1,         VLENGTH = TRUE,
   BETX = BETX0, ALFX = ALFX0,
   DX   = DX0,   DPX  = DPX0,
   BETY = BETY0, ALFY = ALFY0,
   DY   = DY0,   DPY  = DPY0;
  !VARY,  NAME = kqid.12, STEP = 0.001,   LOWER = -0.1, UPPER = 0.0;
  VARY,   NAME = kqif.13, STEP = 0.001,   LOWER = 0.04, UPPER = 0.1;
  VARY,   NAME = kqid.13, STEP = 0.001,   LOWER = -0.1, UPPER = 0.0;
  VARY,   NAME = kqif.14, STEP = 0.001,   LOWER = 0.04, UPPER = 0.071;
  VARY,   NAME = kqid.14, STEP = 0.001,   LOWER = -0.1, UPPER = 0.0;
  VARY,   NAME = kqif.15, STEP = 0.001,   LOWER = 0.04, UPPER = 0.07;
  VARY,   NAME = kqid.15, STEP = 0.001,   LOWER = -0.1, UPPER = 0.0;
  VARY,   NAME = kqif.16, STEP = 0.001,   LOWER =  0.0, UPPER = 0.1;
  VARY,   NAME = kqid.16, STEP = 0.001,   LOWER = -0.1, UPPER = 0.0;
  !VARY,  NAME = MQ.e10.at, STEP = 0.001,  LOWER = 115,  UPPER = 120;
  !VARY,  NAME = MQ.e11.at, STEP = 0.001,  LOWER = 123,  UPPER = 127;
  CONSTRAINT,  RANGE = ps2.omk.foil,  BETX=BETX1,  BETY=BETY1;
  CONSTRAINT,  RANGE = ps2.omk.foil,  ALFX=ALFX1,  ALFY=ALFY1;
  CONSTRAINT,  RANGE = ps2.omk.foil,  DX=DX1,      DPX=DPX1;
  CONSTRAINT,  RANGE = ps2.omk.foil,  DY=DY1,      DPY=DPY1;
LMDIF, CALLS:=5000, TOLERANCE:=1.E-10;
ENDMATCH;
```

Fig. A.3: Example for the matching sections from SPL to FODO and from FODO to PS2, courtesy C. Hessler.

```
corrmacro(nx): macro={

use, sequence=bt1btp;
sigma:=2;
vert:=TGAUSS(2);

EOPTION,SEED=nx,ADD=false;

eps_x=2e-6/2.9676;
delta_p=1.07e-3;

rand_x=gauss(nx);
sigma_x = sqrt(eps_x * betx0);
x0 = 0.015*rand_x *( sigma_x + (abs(dx0) * delta_p));

rand_px=gauss(nx);
px0 = 0.015*rand_px *((sqrt(eps_x / betx0) - (alfx0 / betx0) * sigma_x))
+ (dpx0 * delta_p);

eps_y=2e-6/2.9676;
//delta_p=1.07e-3;

rand_y=gauss(nx);
sigma_y = sqrt(eps_y * bety0);
y0 = 0.01*rand_y * (sigma_y + (abs(dy0) * delta_p));

rand_py=gauss(nx);
py0 = 0.01*rand_py *((sqrt(eps_y / bety0) -
(alfy0 / bety0) * sigma_y)) + (dpy0 * delta_p);
```

Fig. A.4: Example for orbit correction studies: input error

```
EOPTION,ADD= FALSE, SEED:=nx;
SELECT, flag= error, clear;

SELECT, FLAG= ERROR, PATTERN= "BT.BHZ10";
EFCOMP, ORDER:= 0, Radius:=0.01,
DKNR:={5e-4*TGAUSS(sigma),0,0,0,0,0,0,0,0,0,0,0,0,0,0,0,0,0,0,0},
DKSR:={0,0,0,0,0,0,0,0,0,0,0,0,0,0,0,0,0,0,0,0,0};
EALIGN,  DS:= 0.3e-3*TGAUSS(sigma), DX:= 0.3e-3*TGAUSS(sigma),
DY:= 0.3e-3*TGAUSS(sigma), DPHI:= 0.3e-3*TGAUSS(sigma),
DTHETA:= 0.3e-3*TGAUSS(sigma), DPSI:= 0.3e-3*TGAUSS(sigma);
```

Fig. A.5: Example for orbit correction studies: assigning errors to magnets

```
SELECT,FLAG=ERROR,FULL;
ESAVE,FILE='errors.tfs';

select, flag=twiss, clear;
select, flag= twiss, column= s,x,y,betx,bety,px,py;
TWISS,file="outcorr/test/twissnocorr.nx.tfs", deltap= 0.0,
sequence= bt1btp,BETA0=INITBETA0;

option,echo;

COPTION, PRINT=10;

CORRECT, flag = line, PLANE= x, MODE=svd, COND=0, MONON=1,
MONERROR=1, MONSCALE=0, RESOUT=0, ERROR=1.E-6, CORRLIM=1.0,
CLIST=xcorr.nx.out, MLIST=ymon.nx.out;

CORRECT, flag = line, PLANE= y, MODE=svd, COND=0, MONON=1,
MONERROR=1, MONSCALE=0, RESOUT=0, ERROR=1.E-6, CORRLIM=1.0,
CLIST=ycorr.nx.out, MLIST=xmon.nx.out;

select, flag= corr, column= PX.OLD,PY.OLD,PX.CORRECTION,PY.CORRECTION;

select, flag=twiss, clear;
select, flag= twiss, column= s,x,y,betx,bety,px,py;
TWISS,file="outcorr/test/twisscorr.nx.tfs", deltap= 0.0,
sequence= bt1btp,BETA0=INITBETA0;
};

n=0;
while (n < 200) {
  exec, corrmacro($n);
 n= n+1;
}
```

Fig. A.6: Example for orbit correction studies: correction part